

**GALACTIC EVOLUTION OF
D AND ^3He INCLUDING
STELLAR PRODUCTION OF ^3He**

DAVID S. P. DEARBORN¹, GARY STEIGMAN²
AND MONICA TOSI³

arXiv:astro-ph/9601117v1 22 Jan 1996

¹Lawrence Livermore National Laboratory L-58, P. O. Box 808, Livermore, CA 94550

²Departments of Physics and Astronomy, The Ohio State University, 174 West 18th Avenue, Columbus, OH 43210

³Osservatorio Astronomico di Bologna, Via Zamboni 33, 40126 Bologna, ITALY

ABSTRACT

New stellar models which track the production and destruction of ${}^3\text{He}$ (and D) have been evolved for a range of stellar masses ($0.65 \leq M/M_{\odot} \leq 100$), metallicities ($0.01 \leq Z/Z_{\odot} \leq 1$) and initial (main sequence) ${}^3\text{He}$ mass fractions ($10^{-5} \leq X_{3,MS} \leq 10^{-3}$). Armed with the ${}^3\text{He}$ yields from these stellar models we have followed the evolution of D and ${}^3\text{He}$ using a variety of chemical evolution models with and without infall of primordial or processed material. Production of new ${}^3\text{He}$ by the lower mass stars overwhelms any reasonable primordial contributions and leads to predicted abundances in the presolar nebula and/or the present interstellar medium in excess of the observationally inferred values. This result, which obtains even for zero primordial D and ${}^3\text{He}$, and was anticipated by Rood, Steigman & Tinsley (1976), is insensitive to the choice of chemical evolution model; it is driven by the large ${}^3\text{He}$ yields from low mass stars. In an attempt to ameliorate this problem we have considered a number of non-standard models in which the yields from low mass stars have been modified. Although several of these non-standard models may be consistent with the ${}^3\text{He}$ data, they may be inconsistent with observations of ${}^{12}\text{C}/{}^{13}\text{C}$, ${}^{18}\text{O}$ and, most seriously, the super- ${}^3\text{He}$ rich planetary nebulae (Rood, Bania & Wilson 1992). Even using the most extreme of these non-standard models (Hogan 1995), we obtain a generous upper bound to pre-galactic ${}^3\text{He}$: $X_{3P} \leq 3.2 \times 10^{-5}$ which, nonetheless, leads to a stringent lower bound to the universal density of nucleons.

1. INTRODUCTION

To test and constrain models of primordial nucleosynthesis it is necessary to confront the predicted abundances with observational data. Such comparisons are complicated by the necessity of extrapolating the abundances inferred “here and now” (solar system, ISM, etc.) to their “there and then” (primordial or pregalactic) universal values. This difficulty is somewhat ameliorated for ^4He which is observed in less evolved, low metallicity extragalactic HII regions (e.g., Pagel et al. 1991; Skillman et al. 1994; Olive & Steigman 1995) and for ^7Li which is probed in metal poor halo stars (Spite & Spite 1982; Thorburn 1994). In contrast, ^3He is only observed in the solar system (Black 1971, 1972; Geiss & Reeves 1972; Geiss 1993) and in Galactic HII regions (Bania, Rood & Wilson 1987; Balser et al. 1994). Until recently, D, too, had only been observed “here and now”. A new era in probing deuterium has dawned with the identification of possible absorption of QSO light by high redshift D (Carswell et al. 1994; Songaila et al. 1994; Tytler 1995). However, “wrong velocity” hydrogen absorbers may masquerade as deuterium (Carswell et al. 1994; Songaila et al. 1994; Steigman 1994) so that much more data are required before such observations may be used to fix the nearly primordial abundance of D. Thus, to infer the pregalactic abundances of D and ^3He it is currently necessary to have recourse to models of galactic chemical evolution. Unfortunately, the uncertainties and/or lack of uniqueness of such models compound the observational uncertainties.

The evolution of D is straightforward since when incorporated in a star it is burned (to ^3He) during the pre-main sequence evolution. If the “virgin” fraction of the ISM (either today or at the time of formation of the solar system 4.5 Gyr ago) were known, the primordial D abundance could be inferred from ISM or solar system observations. A very large class of chemical evolution models (Audouze & Tinsley 1974; Tosi 1988 a,b; Vangioni-Flam & Audouze 1988; Matteucci & François 1989; Steigman & Tosi 1992), constrained by heavy element abundances, abundance gradients, abundance ratios (primary vs. secondary) and cosmochronometers, find that $\sim 1/3 - 2/3$ of the ISM (now, t_0 or, at the time of the solar system formation, t_\odot) has never been through stars. However, “designer models” with larger D destruction (Vangioni-Flam, Olive & Prantzos 1994; Olive et al. 1995; Scully & Olive 1995) do exist (but see, e.g., Edmunds 1994 and Prantzos 1995 for their consistency problems).

The galactic evolution of ^3He is complex. Any prestellar ^3He is enhanced by the pre-main sequence burning of prestellar D. Thus, when a star reaches the main sequence the ^3He mass fraction exceeds that in the prestellar nebula [$X_{3,MS} = (X_3 + 3X_2/2)_{pre}$; in what follows we write X_i for mass fractions and y_i for ratios by number to hydrogen; $y_{ij} \equiv y_i + y_j$]. ^3He survives nuclear burning in the cooler outer layers of stars, is destroyed in the hotter interiors and, especially in low mass stars, is synthesized via hydrogen burning. Thus, depending on the mass (and, to a lesser extent the metallicity) of a star, ^3He is preserved, produced or destroyed. To understand the galactic evolution of ^3He , it is necessary to first understand its stellar evolution (Iben 1967; Rood 1972; Dearborn, Schramm & Steigman 1986; Vassiliadis & Wood 1993). However, since *some* ^3He survives stellar processing and,

prestellar D is burned to ${}^3\text{He}$, the evolution of ${}^3\text{He}$ (or, $\text{D} + {}^3\text{He}$) is less rapid than that of D alone (Yang et al. 1984; hereafter YTSSO). Thus, observations of D and ${}^3\text{He}$ (e.g., in the solar system) may be used to infer an *upper bound* to primordial D and/or $\text{D} + {}^3\text{He}$ (YTSSO; Walker et al. 1991; hereafter WSSOK). As a result, models which destroy D more efficiently are to some extent constrained by the requirement that solar system and/or ISM ${}^3\text{He}$ not be overproduced.

Rood, Steigman & Tinsley (1976; hereafter RST) first included stellar production of ${}^3\text{He}$ in numerical models of galactic evolution. RST found that stellar production led to a rapid increase in X_3 from t_{\odot} to t_0 which seemed in conflict with the then current observations (only bounds) and concluded that it seemed unlikely that ${}^3\text{He}$ could be used cosmologically. As we shall see, this problem persists today (Olive et al. 1995).

In a previous study (Steigman & Tosi 1992; hereafter ST92) we used the ${}^3\text{He}$ survival from Dearborn, Schramm & Steigman (1986) in models of galactic evolution consistent with a large number of observational constraints (Tosi 1988a) to track the evolution of D and ${}^3\text{He}$. Not including ${}^3\text{He}$ production in low mass stars, we found that $X_{3P} \approx X_{3\odot} \approx X_{30}$ for a wide range of choices of initial (primordial) abundances for D and ${}^3\text{He}$. Similar results have been found, e.g., by Fields (1995). At the same time, the ${}^3\text{He}$ HII region data (Bania, Rood & Wilson 1987; Rood, Bania & Wilson 1992) have been supplemented by new and important observations of super- ${}^3\text{He}$ rich material in a few planetary nebulae (Balsler et al. 1994, Rood et al. 1995, hereinafter RBWB95). Since the gas in PNe reflects the chemical composition of the ejected outer layers of their central stars, where the original ${}^3\text{He}$ abundance has certainly been modified by stellar processing, their large ${}^3\text{He}$ abundances should not be taken as representative of the ISM abundances at the time of the formation of their central stars but, of the effect of stellar nucleosynthesis in low mass stars. The observed abundances lend support to the estimates of newly synthesized ${}^3\text{He}$ ($X_{3*} \approx 0.7 - 7 \times 10^{-3}$) in low mass stars ($0.6 - 2.3M_{\odot}$) in the pioneering work of Iben (1967) and Rood (1972) and makes timely a reinvestigation of the galactic evolution of ${}^3\text{He}$ (along with D) *including* stellar production of ${}^3\text{He}$ (Galli et al. 1995, Tosi, Steigman & Dearborn 1995, Olive et al. 1995). To this aim, we have computed an extensive grid of stellar evolution models with varying initial abundances of ${}^3\text{He}$ and of the overall metallicity Z , and we have reexamined the galactic evolution of D and ${}^3\text{He}$ in the framework of such stellar models.

In §2 we describe the stellar models we’ve evolved to follow the evolution of ${}^3\text{He}$ and present our results for the survival/production of ${}^3\text{He}$ as a function of stellar mass ($0.65 \leq M/M_{\odot} \leq 100$), metallicity ($Z = 0.02, 0.002, 0.0002$) and initial (“main sequence” $\Rightarrow \text{D} + {}^3\text{He}$) ${}^3\text{He}$ ($10^5 X_{3,MS} = 1.0, 5.0, 10, 21, 100$). In §3 and §4 we use the stellar results in a series of chemical evolution models (Tosi 1988a,b; ST92) to follow the galactic evolution of D and ${}^3\text{He}$. In §5 we further follow the ${}^3\text{He}$ evolution modifying the stellar yields. Sections 6 & 7 are reserved for discussions and conclusions.

2. STELLAR EVOLUTION OF ${}^3\text{He}$

The evolution of stars with $M = 0.65M_{\odot}$ to $M = 100M_{\odot}$ and three metallicities (“Pop I”: $X = 0.70$, $Z = 0.02$, “Pop I 1/2”: $X = 0.76$, $Z = 0.002$, “Pop II”: $X = 0.76$, $Z = 0.0002$) was followed using the code described in Dearborn, Griest & Raffelt (1991) which is derived from that of Eggleton (1967, 1968). OPAL opacities (Iglesias & Rogers 1990, 1992) are used for temperatures above 6000K and Los Alamos opacities (Heubner et al. 1977), including the contribution of molecules, for lower temperatures. Our code follows ${}^3\text{He}$ production and destruction in all hydrogen burning regions and a post-processor is used to calculate the nucleosynthesis of D and the isotopes of Li, Be, C, N, O and several other elements. Calculations with this post-processor confirmed the pre-main sequence conversion of D to ${}^3\text{He}$. The mixing length is chosen to give the correct solar radius and this model predicts a neutrino flux (for the chlorine experiment) of 7.9 SNU and the p-mode spectrum matches that of Bahcall & Ulrich (1988). For the Pop I 1/2 and Pop II models, a slightly larger mixing length is required to fit the color-magnitude data for M30 (Bolte 1994). However, ${}^3\text{He}$ evolution is insensitive to any reasonable choice of mixing length.

All models began in the pre-main sequence on the Hayashi track. The final evolutionary state depended on the mass of the star. Stars with $0.65 \leq M/M_{\odot} \leq 2.00$ were evolved up to the helium flash. For one model ($1.5M_{\odot}$) the evolution was followed through the helium flash and up the asymptotic giant branch (AGB). This additional evolution (without thermal pulses) changed the ${}^3\text{He}$ mass fraction in the envelope by less than 1%, demonstrating that in the absence of thermal pulses, the envelope abundance of ${}^3\text{He}$ is insensitive to the subsequent (post helium flash) evolution of these stars. Intermediate mass stars ($2.5 \leq M/M_{\odot} \leq 8.0$) were all evolved to the AGB, to a point where mass loss (and possibly Planetary Nebula formation) dominates their remaining evolution. All massive star models ($M \geq 10M_{\odot}$) were evolved into carbon burning and are within a few thousand years of core collapse, leaving insufficient time for significant changes in the composition of their hydrogen envelopes. We have not allowed for winds and this suggests that, for the more massive stars, we have underestimated the ${}^3\text{He}$ returned to the ISM (see, e.g., Dearborn, Schramm & Steigman 1986).

Since D is completely burned to ${}^3\text{He}$ in the pre-main sequence, our “main sequence” (MS) ${}^3\text{He}$ abundance reflects the prestellar contribution from D and ${}^3\text{He}$: $X_{3,MS} = X_3 + 3X_2/2$. To explore the sensitivity of our ${}^3\text{He}$ yields (envelope fractions $X_3(env)$) to $X_{3,MS}$ we have chosen five values of $X_{3,MS}$ from 1×10^{-5} to 1×10^{-3} . The top panel of Figure 1 shows our Pop I yields $X_{3f} \equiv X_3(env)$ as a function of the initial stellar mass for different choices of $X_{3,MS}$. For lower mass stars production dominates and, when convection on the giant branch homogenizes the envelope, the ${}^3\text{He}$ available to be returned to the ISM is strongly enhanced. Without substantial mass loss, these lower mass stars remain near the Hayashi track during helium burning and beyond. In the absence of a hot bottom convection zone stimulated by thermal pulses, there is no destruction of this “new” ${}^3\text{He}$. For more massive stars the lifetimes are shorter resulting in less ${}^3\text{He}$ production in the temperature regimes where this occurs. Note that if these stars started with no initial ${}^3\text{He}$ they would, in fact,

be net producers of ${}^3\text{He}$; in this case $g_3 \equiv X_{3f}/X_{3,MS}$ would diverge. However, for the range of $X_{3,MS}$ of interest ($10^{-5} - 10^{-3}$), the small production of ${}^3\text{He}$ in more massive stars does not compensate for the destruction of initial ${}^3\text{He}$.

A striking feature of the 15 and $25M_{\odot}$ Pop I models is the dip in X_{3f} . The high envelope opacity allowed these models to homogenize the envelope on the giant branch prior to helium burning. The blue loop that occurred during helium burning then led to a second epoch of ${}^3\text{He}$ destruction. In contrast, the 50 and $100M_{\odot}$ models completed their helium burning before evolving to the red thus leading to the “recovery” of X_{3f} seen in the top panel of Figure 1. Similarly, the lower metallicity ($Z=0.002$ and $Z=0.0002$) $25M_{\odot}$ models did not evolve all the way to the red giant branch prior to helium burning and, therefore, these stars only experienced ${}^3\text{He}$ destruction on the main sequence (see bottom panel of Fig.1). For Pop I 1/2 and Pop II stars the lower opacity results in a more compact, warmer structure (similar to that of a slightly more massive Pop I star). At a fixed mass this leads to a shorter lifetime resulting in less production and more destruction of ${}^3\text{He}$. However, the lower metallicity 15 & $25M_{\odot}$ models do not experience a second epoch of ${}^3\text{He}$ destruction. As a result, they show less ${}^3\text{He}$ destruction than the Pop I models (i.e., no dip in X_{3f} vs. $X_{3,MS}$). By comparing the two panels of Fig.1, it is apparent that the amount of ${}^3\text{He}$ ejected by stars depends much more on its main sequence ${}^3\text{He}$ abundance than on the overall stellar metallicity.

In Figure 2 we display our $Z=0.02$ (Pop I) results from a different perspective by showing the final yield (X_{3f}) as a function of the initial abundance ($X_{3,MS}$) for $1 \leq M/M_{\odot} \leq 100$. For $M = 1M_{\odot}$, production dominates and X_{3f} is (nearly) independent of $X_{3,MS}$ (except at the highest $X_{3,MS}$). In contrast, for $M = 100M_{\odot}$ production is negligible and X_{3f} varies linearly with $X_{3,MS}$. The transition from low to high mass models is seen for $M = 3$ and $8M_{\odot}$. For $0.65 \leq M/M_{\odot} \leq 2.5$, where production dominates, we find $X_{3f} \approx (M_{\odot}/M)^{2.2} \times 10^{-3}$. For more massive stars the relation between X_{3f} and $X_{3,MS}$ is more complex. As $X_{3,MS}$ increases, ${}^3\text{He}$ production is relatively less important resulting in the curvature seen in Figure 2 for $M = 3$ and $8 M_{\odot}$. For high masses where production is negligible, $X_{3f} \approx 0.33X_{3,MS}$.

In the absence of ${}^3\text{He}$ production it is interesting to consider the ${}^3\text{He}$ “survival fraction” $g_3 \equiv X_{3f}/X_{3,MS}$ (Dearborn, Schramm & Steigman 1986; YTSSO; ST92). In the presence of ${}^3\text{He}$ production g_3 is less useful and, potentially misleading since the yield is not proportional to $X_{3,MS}$. Nonetheless, for comparison with previously published results, g_3 vs. M for our five choices of $X_{3,MS}$ is shown in Figure 3. The divergence of the curves at low M reflects the increasing importance of ${}^3\text{He}$ production which sets in first (at the largest M) for the lowest values of $X_{3,MS}$. Note that in the limit that $X_{3,MS}$ goes to zero, g_3 diverges. In Figure 4 is shown $\langle g_3 \rangle$, the value of g_3 averaged over Tinsley’s (1980) IMF as a function of the lower mass limit m_l of the IMF. For gas incorporated in a generation of stars, as time increases material is returned from lower mass stars and so Fig. 4 provides a picture of the time-evolution of the ${}^3\text{He}$ “survival”. Note that for all m_l , $\langle g_3 \rangle \gtrsim 0.3$. Depending on the initial abundance, production dominates, $\langle g_3 \rangle \gtrsim 1$, for m_l up to $7M_{\odot}$. In terms of galactic

evolution this implies that the ISM starts to be enriched in ^3He as soon as stars less massive than $3 - 7M_{\odot}$ (depending on the initial ^3He abundance) start to die. We note again that stars above $\sim 25M_{\odot}$ are likely to experience mass loss which will return unburnt ^3He to the ISM. For massive stars our neglect of mass loss results in an underestimate of g_3 .

The trends in our results are easy to understand. During the hydrogen burning phase ^3He is produced in the core of stars of all masses. However, with time, the core temperature (which depends on stellar mass) increases to values where ^3He is burned. Thus, new ^3He survives only in a radiative shell adjacent to the convective core and, from this shell, may later be dredged up to the surface where it will mix with the prestellar (MS) ^3He . The competition between net production or destruction then depends not only on $X_{3,MS}$ but, on the size of the shell and the amount of new ^3He there, and on the depth of the dredge-ups (i.e., do they bring to the surface material which is enhanced or depleted in ^3He). In low mass stars much new ^3He is produced and most of it survives to dominate over (reasonably small values of) $X_{3,MS}$. In contrast, for massive stars little new ^3He is synthesized in the core, destruction is efficient and the ^3He preservation shell is small so that the initial ^3He dominates.

We note that the Eggleton type code we use permits larger time steps on the AGB which tends to suppress thermal pulses. However, when short timesteps are enforced, these pulses occur. Such pulses are plausible sites for the lithium enhancements – produced at the expense of ^3He – observed in some S-type stars. Although it doesn't require much ^3He depletion to yield huge lithium enhancements, since the lithium is fragile it is possible that the lithium enhancement attains a steady state with ^3He processed to ^4He . A limit on such ^3He processing might follow from the fact that a very fragile nucleus, ^{18}O , survives the dredge up in normal carbon stars (Dearborn 1992). Since ^3He is destroyed at higher temperatures than those for ^{18}O , the lack of ^{18}O depletion suggests that ^3He is not strongly depleted in normal carbon stars.

A similar argument applies to the main sequence mixing proposed to explain the low $^{12}\text{C}/^{13}\text{C}$ ratios observed in red giants (Dearborn & Eggleton 1976; Dearborn 1992). In red giants ^{18}O appears to be independent of the ^{13}C enhancement, perhaps due to stabilization by a molecular weight gradient. Since it is difficult to mix with a region of depleted ^3He without modifying ^{18}O , it is suggestive that ^3He is not destroyed in these stars. In contrast, J-type carbon stars have CNO-equilibrium values for $^{12}\text{C}/^{13}\text{C}$ and do show ^{18}O depletions. In such stars ^3He is likely destroyed throughout the envelope. If most carbon stars pass through such a stage (rather than these representing a separate class of stars), little ^3He may survive. Pinsonneault (Private Communication) has noted that for solar metallicity stars, the open cluster M67 seems to be the dividing line between stars which do not undergo giant branch mixing and those which do suggesting that mixing for stars with $M \gtrsim 1.3 - 1.5M_{\odot}$ is inconsistent with the $^{12}\text{C}/^{13}\text{C}$ data.

It is interesting to compare our results with the recent work of Vassiliadis & Wood (1993). We both agree that in the low mass stars there is no significant change in ^3He between the first and second dredge up. Further, Vassiliadis & Wood calculate thermal

pulses and, for stars below 5 solar masses, they find no change in the ^3He abundance. Our mixing length approximations are nearly the same and they included a wind which stripped the envelope on the AGB while we did not. Quantitatively, our yields and theirs are in excellent agreement (provided that their $\theta(^3\text{He})$ is a mass fraction) despite the fact that their opacities are different (higher) than ours and they used slightly older nuclear reaction rates.

3. THE GALACTIC EVOLUTION OF D

As in ST92 we have followed the evolution of D and ^3He for the two “best” chemical evolution models for the galactic disk identified in Tosi (1988a) along with a third model in which, for comparison, infall is absent. Model 1, the “best” model (Tosi 1988a; Giovagnoli & Tosi 1995), consistent with the major observational constraints, has an exponentially decreasing SFR (with a 15 Gyr e-folding time), depending on both the gas and total mass density currently observed in each ring, a constant (in time), uniform (in space) infall rate of $0.004 M_{\odot}/kpc^2/yr$ and uses Tinsley’s (1980) IMF. Model 25, the “second best” model (Tosi 1988a) also has an exponentially decreasing SFR with, however, a 5 Gyr e-folding time, an effectively constant (e-folding time of 100 Gyr) infall rate of uniform density $0.002 M_{\odot}/kpc^2/yr$ and Tinsley’s (1980) IMF. Our comparison No Infall (NI) model uses the same IMF and SFR e-folding time as Model 1 but is normalized so as to reproduce the current SFR and gas/total mass distributions with galactocentric distance. We recall, however, that such a model does not reproduce the major features (distribution with time and galactocentric distance of the chemical abundances) observed in the galactic disk.

Normally, our models adopt 13 Gyr for the present epoch and 8.5 Gyr for the formation of the solar system. To explore the sensitivity to the age of the model, we have run some models (indicated by a subscript 10) where the present epoch is 10 Gyr and solar system formation is at 5.5 Gyr.

Since infall plays an important role in Models 1 & 25, it is necessary to specify the chemical composition of the infalling gas. We have considered models with primordial infall ($Z_{infall} = 0$) for which $X_{2infall} = X_{2P}$ and $X_{3infall} = X_{3P}$ as well as models with partially processed infalling material. In the latter cases we have adopted $Z_{infall} = 0.2Z_{\odot}$, a value low enough to preserve the infall dilution efficiency and keep the model predictions in agreement with the observational constraints in the solar neighbourhood and in the whole disk (Tosi 1988b, Matteucci & François 1989). When $Z_{infall} = 0.2Z_{\odot}$, the infall abundance of D is certainly lower than primordial due to stellar processing, whereas the ^3He abundance in principle can be either lower or higher depending on the mass of the stars contributing to the enrichment of the accreted gas. We have thus considered models with $X_{2infall} = 0.7X_{2P}$ or $X_{2infall} = 0.8X_{2P}$ and $X_{3infall} = 0.8X_{3P}$ or $X_{3infall} = X_{3P}$ or $X_{3infall} = 1.2X_{3P}$. From a series of model checks we find that larger deviations of the infall abundances of D from the primordial value would be rather improbable with an overall metallicity $Z_{infall} = 0.2Z_{\odot}$.

To explore the sensitivity of our results to the primordial values we have run each model for a range of choices of X_{2P} and X_{3P} ($0 \leq 10^5 X_{2P} \leq 9.0$; $0 \leq 10^5 X_{3P} \leq 4.0$). In Table 1 we list the set of models explored.

The evolution of deuterium is straightforward since any D incorporated in stars is destroyed. Thus, the D survival factor, $f_2 = X_2/X_{2P}$, is identical to the fraction of the ISM that has never been through stars. f_2 , then, is independent of X_{2P} and purely reflects the chemical evolution model. In Figure 5 we show f_2 evaluated at the solar ring ($R = 8kpc$) as a function of time. For each model (1 & 25) we show the differences between primordial infall ($Z_{infall} = 0$, $X_{2infall} = X_{2P}$) and non-primordial infall ($Z_{infall} = 0.2Z_{\odot}$, $X_{2P} = 0.8X_{2P}$) as well as the corresponding no-infall (NI) model. We also compare in Figure 5 models whose present age is 13 Gyr with 10 Gyr models. The models with non-primordial infall have less D refueling of the ISM and show a steeper decrease with time of f_2 than models with primordial infall. The NI model destroys D more slowly at first but, without replenishment of ISM D via infall, eventually has the largest D depletion. The short lifetime models (10 Gyr) have less time to destroy D but, to reproduce present observations have higher initial mass and SFR than the 13 Gyr models. The net result of this balancing act is that the 10 Gyr (infall) models have higher $f_{2\odot}$ but lower f_{20} ; the NI models have larger f_2 correlating with lower age. For Models 1 & 25 the entire ranges are: $0.49 \leq f_{2\odot} \leq 0.73$; $0.43 \leq f_{20} \leq 0.62$; for the NI models: $0.70 \leq f_{2\odot} \leq 0.78$; $0.30 \leq f_{20} \leq 0.36$. Thus, for our range of models D astration is modest, typically by a factor of 1.3 to 2.0 at t_{\odot} and a factor of 1.6 to 3.3 at t_0 . Our Models 1 & 25 have very little evolution in f_2 from t_{\odot} to t_0 ($0.9 \leq f_{20}/f_{2\odot} \leq 1.2$ for $t_0 = 13$ Gyr; $1.3 \leq f_{20}/f_{2\odot} \leq 1.5$ for $t_0 = 10$ Gyr). This is entirely consistent with the solar system and ISM data: $X_{20}/X_{2\odot} = 1.6 \pm 0.6$ (e.g., Steigman & Tosi 1995).

In Figure 6 we show the time evolution of X_2 in the solar ring for Models 1, 25 & NI for $t_0 = 13, 10$ Gyr. Also shown in Figure 6 are the 2σ ranges of the solar system (Geiss 1993; Steigman & Tosi 1995) and ISM (Linsky et al. 1992; Steigman & Tosi 1995) D abundances. For Models 1 & 25 the ISM constraint dominates, limiting primordial D to $X_{2P} \leq 6 \times 10^{-5}$ (for $Y_P \lesssim 0.25$, $y_{2P} \lesssim 4 \times 10^{-5}$). Even for the NI model we find a restrictive bound $X_{2P} \leq 9 \times 10^{-5}$ ($y_{2P} \lesssim 6 \times 10^{-5}$).

In Figure 7 is shown the predicted radial distribution of D/H at present. The positive gradient is a natural consequence of larger D destruction in regions with larger SFR. The “data” are from Wannier (1980) *but* have been *divided by a factor of 100* to facilitate comparison; while they appear to reflect the expected radial distribution, they are some two orders of magnitude *too large*, possibly due to the chemical fractionation of deuterated molecules.

With the adoption of a chemical evolution model (e.g., 1, 25 or NI; $t_0 = 13$ or 10 Gyr; $X_{2infall}/X_{2P} = 1.0$ or 0.8) the evolution of deuterium (with time and location in the Galaxy) is completely determined. Comparison with solar system and ISM observations then fixes (bounds) the primordial D abundance. For our “normal” models (not the NI models) we find $2.7 \leq 10^5 X_{2P} \leq 6.6$ (for $X_P \gtrsim 0.75$, $1.8 \lesssim 10^5 y_{2P} \lesssim 4.4$) which, for standard big bang nucleosynthesis (Walker et al. 1991; Thomas et al. 1995) bounds the nucleon-to-photon

ratio η : $4.1 \lesssim \eta_{10} \lesssim 7.1$ ($\eta_{10} = 10^{10}\eta = 10^{10}n_N/n_\gamma$). Our (artificial) NI models prefer somewhat higher primordial D: $4.7 \leq 10^5 X_{2P} \leq 8.8$ ($3.2 \lesssim 10^5 y_{2P} \lesssim 5.9$; $3.5 \lesssim \eta_{10} \lesssim 5.1$). The modest astration we find is similar to many previous results (Audouze & Tinsley 1974; ST92; Galli et al. 1995; Fields 1995). Nonetheless, it may be possible to construct chemical evolution models with more destruction of D although consistency with all the observational constraints is quite improbable (Vangioni-Flam & Audouze 1988; Vangioni-Flam, Olive & Prantzos 1994; Olive et al. 1995; Olive & Scully 1995). An important test of all models is the evolution of ${}^3\text{He}$ (RST).

4. THE GALACTIC EVOLUTION OF ${}^3\text{He}$: STANDARD MODELS

The evolution of ${}^3\text{He}$ is much more complex than that of D since ${}^3\text{He}$ may be destroyed, preserved and produced in differing proportions in stars of differing masses. Here, we have used the stellar results described in §2 in concert with the large number of models summarized in Table 1. The key difference with our earlier work (ST92), which utilized similar models, is our allowance here for the production of new ${}^3\text{He}$ synthesized in lower mass stars. Following the results of §2, in running the models, at each time step the adopted stellar yields are those corresponding to the X_{3f} of the dying stars. As anticipated by RST, the effect of ${}^3\text{He}$ production is large, dominating the evolution of ${}^3\text{He}$.

In Figure 8 the evolution of ${}^3\text{He}$ is shown for a wide variety of choices of X_{2P} , X_{3P} , X_{2inf} , X_{3inf} for Model 1 and a present age of 13 Gyr. The vertical bar at 8.5 Gyr corresponds to the 2σ range of abundances derived in the solar system (Geiss 1993). Given the lack of ${}^3\text{He}$ determinations for the local ISM, the vertical bar at 13 Gyr corresponds to the 2σ range of abundances derived by RBWB95 for HII regions between 6.4 and 10.3 kpc from the galactic center (but excluding W3 which definitely lies outside the average distribution and is the worst case for pressure broadening corrections). In the upper panel of Figure 8, the problem of excessive ${}^3\text{He}$ production identified by RST is clear. Using the stellar yields from §2, it may be seen that there are **no** choices of X_{2P} and X_{3P} consistent with the range of ${}^3\text{He}$ abundances inferred from the solar system and/or ISM data. After the first few Gyr of evolution the contribution from newly synthesized ${}^3\text{He}$ overwhelms any primordial D+ ${}^3\text{He}$ and, even when $X_{2P} = X_{3P} = 0$, the ${}^3\text{He}$ abundances after 8.5 (13) Gyr are in excess of the solar system and ISM upper bounds.

The trends displayed in the upper panel of Figure 8 are easy to understand. For fixed choices of X_{3P} , $X_3(t)$ increases with increasing X_{2P} since any prestellar D is burned to ${}^3\text{He}$, enhancing the main sequence abundance of ${}^3\text{He}$. Models which begin with higher X_{3P} always have higher ${}^3\text{He}$ abundances although, with time, the differences are reduced by the emerging dominance of the newly synthesized ${}^3\text{He}$.

The upper four curves in the bottom panel of Figure 8 demonstrate the effect of the different choices for the infall abundances. However, these differences are small compared to the overall enhancement by stellar produced ${}^3\text{He}$. As in the upper panel, even in the

absence of any primordial D or ^3He , the predicted ^3He abundances at the time of formation of the solar system and/or at present are in excess of the observational upper bounds.

Thus, our results confirm - with a vengeance - the RST identified problem of ^3He overproduction when the contribution of new ^3He from low mass stars is included in models of galactic chemical evolution (see also Galli et al. 1995). This conclusion is not modified when we used Model 25, the NI model or, for any of these models with a 10 Gyr disk age. We have, therefore, considered how we might have to modify the contribution of new ^3He from the low mass stars in order to reconcile ^3He evolution with the observational data.

5. THE GALACTIC EVOLUTION OF ^3He : NON-STANDARD MODELS

As outlined in Table 1, in addition to our standard models (with the yields from §2), we have considered several non-standard models by modifying the ^3He yields from low mass stars. As may be seen from the bottom panel of Figure 8 and in both panels of Figure 9, there are a variety of possible solutions to the problem of ^3He overproduction. The rapid increase in ^3He is most curtailed in models VI which follow the suggestion of Hogan (1995) that in stars less than $2.5 M_{\odot}$, ^3He is destroyed on the giant branch before it can be returned to the ISM and the final envelopes of these stars therefore only contain an abundance X_{3f} corresponding to the equilibrium value $^3\text{He}/\text{H}=1\times 10^{-5}$. However, Hogan's (1995) suggestion is in conflict with the normal $^{12}\text{C}/^{13}\text{C}$ ratios observed in stars more massive than $1.3\text{-}1.5 M_{\odot}$ (Pinsonneault, Private Communication), as well as the observations of lithium (more fragile than ^3He) in some of them. Even worse, the observations of excess ^3He (X_3 of order 10^{-3}) in three planetary nebulae (Rood, Bania & Wilson 1992; RBWB95) appear to confirm that stars around $1.5 M_{\odot}$ are efficient ^3He producers, in conflict with Hogan's proposal. Charbonnel (1995) has recently argued that the deep convective mixing responsible for the ^3He destruction in Hogan's suggestion takes place in stars experiencing the helium flash and gives an upper mass limit of $2 M_{\odot}$ to the phenomenon. This would reconcile the deep mixing ^3He destruction with the high PNe abundances if the initial mass of the PNe progenitor was at least $2 M_{\odot}$. However, the three well studied PNe have presumably originated from stars of initial mass $1.5 M_{\odot}$ (Stanghellini, 1995 private communication), thus lying in the range of stellar masses which should deplete and not enhance ^3He in the deep mixing hypothesis.

To try to retain some of the benefit manifest in models VI, we have allowed ^3He to be reduced to its equilibrium value in lower mass stars ($\leq 1 M_{\odot}$ in models V, as suggested by Pinsonneault, 1995, private communication; and $\leq 1.6 M_{\odot}$ in models VII). However, since such low mass stars have long lifetimes, the reduction in ^3He is only effective during recent epochs; solar system ^3He is still overproduced in both cases V and VII (see bottom panel of Fig.8 where the two curves are so close that only one is shown). Even assuming a total ^3He destruction in stars below $1 M_{\odot}$ (i.e. $X_{3f}=0$, case IV) does not solve this inconsistency, since it provides results indistinguishable from case V.

Any other case, with upper mass cutoff for Hogan’s ${}^3\text{He}$ destruction intermediate between 1 and 2.5 would either be inconsistent with the large abundance observed in PNe (if the cutoff is larger than $1.6 M_{\odot}$) or inconsistent with the “low” solar system abundances (if it is smaller than $2 M_{\odot}$). We have therefore tested some models assuming that ${}^3\text{He}$ is reduced to its equilibrium value in stars with mass between an arbitrary lower cutoff and $2.5 M_{\odot}$. If the lower mass cutoff is around $1.3 M_{\odot}$ (case VIII), smaller mass stars still produce large ${}^3\text{He}$ consistent with that observed in PNe and the ISM abundances predicted at the various epochs are consistent with the corresponding observed values (see Figs 8 and 9).

In the models labelled II and III we have - arbitrarily - ignored new ${}^3\text{He}$ production and set $g_3 = 1$ for M below $2 M_{\odot}$ (case II) or, between 1 and $2 M_{\odot}$ (case III; see, e.g., Wasserburg, Boothroyd & Sackmann 1995). As may be seen in Figure 8, models III are consistent with solar system and ISM data provided that the primordial abundances of D and/or ${}^3\text{He}$ are not too large.

Although some of the non-standard models II-VIII may avoid overproduction of presolar and/or ISM ${}^3\text{He}$ the spatial distribution of ${}^3\text{He}$ observed in galactic HII regions (Bania, Rood & Wilson 1987; Rood, Bania & Wilson 1992; Balsaer et al. 1994; RBWB95) provides an important constraint on all such models. The data are puzzling (see, e.g., Olive et al. 1995), exhibiting no very well defined trend of ${}^3\text{He}/\text{H}$ with galactocentric distance R (see Figure 10). Indeed, in contrast to the theoretical expectation that ${}^3\text{He}/\text{H}$ should decrease with R (where the SFR is highest - in the inner galaxy - ${}^3\text{He}/\text{H}$ should also be highest), the data hint at the opposite trend (see Figure 10) typical of elements like H and D which are destroyed and not produced by stellar nucleosynthesis. The only models which avoid a decreasing ${}^3\text{He}$ vs. R relation are those with case VI yields, but cases II and, perhaps, III and VIII may also be consistent with the observed radial distribution, once all the uncertainties are taken into account.

We note that, despite the apparent conflicts of Hogan’s (1995) suggestion with the ${}^{12}\text{C}/{}^{13}\text{C}$, lithium and planetary nebulae data, comparison between case VI and the observational data still leads to a significant upper bound to primordial ${}^3\text{He}$. For case VI we find that $X_{3\odot}/X_{3P} = 1.4$ so that for $X_{3\odot} \leq 4.5 \times 10^{-5}$ (Geiss 1993; ST95), $X_{3P} \leq 3.2 \times 10^{-5}$ ($y_{3P} \leq 1.4 \times 10^{-5}$).

6. DISCUSSION

The evolution of deuterium depends solely on the chemical evolution model, and the D survival fraction, $f_2(t)$, is independent of the primordial abundance and of any stellar uncertainties since D is fully destroyed during the pre-main sequence evolution. For our “best” models (1 & 25; Tosi 1988a,b), D is destroyed by only a modest factor (1.4 - 2.0) by the time of formation of the solar system and, by a slightly larger factor (1.6 - 2.4) up

to the present epoch. Although the artificial NI models permit somewhat more destruction (by a factor of 2.8 - 3.3) by the present epoch, they actually destroy less D (1.3 - 1.4) up to the time of the formation of the solar system. The solar system and ISM data (Geiss 1993; Linsky et al. 1992) may be used along with models 1 & 25 (for a present age of either 10 or 13 Gyr) to bound (at the 95% CL) the primordial D abundance: $2.7 \leq 10^5 X_{2P} \leq 6.6$ ($1.8 \leq 10^5 y_{2P} \leq 4.4$). Comparing to the predictions of BBN (e.g., WSSOK) permits us to bound the universal ratio of nucleons to photons: $4.1 \leq \eta_{10} \leq 7.1$. For our more extreme NI models we find: $4.7 \leq 10^5 X_{2P} \leq 8.8$ ($3.2 \leq 10^5 y_{2P} \leq 5.9$) and $3.5 \leq \eta_{10} \leq 5.1$.

In contrast to D, the evolution of ^3He is much more sensitive to the details of the chemical evolution model and, especially, to the physics of stellar structure and evolution. A key component in our analysis here has been the computation of a new and extensive grid of stellar models covering a wide range of masses ($0.65 \leq M/M_\odot \leq 100$), heavy element abundances ($0.01 \leq Z/Z_\odot \leq 1$) and initial (main sequence) ^3He abundances ($10^{-5} \leq X_{3,MS} \leq 10^{-3}$). We have then followed the ^3He evolution for models 1, 25 & NI with several choices for the present age of the disk (10 & 13 Gyr) and for the chemical composition of the infalling gas ($0.7 \leq X_{2inf}/X_{2P} \leq 1.0$; $0.8 \leq X_{3inf}/X_{3P} \leq 1.2$). As anticipated by RST, after the first few Gyr of evolution, stellar production of ^3He dominates (see, e.g., Figure 8). This contribution from newly synthesized ^3He quickly overwhelms the primordial contribution and, even in the absence of any primordial ^3He (and D), we predict solar system and ISM ^3He abundances in excess of those inferred from the observational data (see also Galli et al. 1995, Tosi et al. 1995). Clearly, there is a problem and, until this conflict is resolved, ^3He cannot serve as a probe of BBN (RST). The problem may lie with the observational data and/or its interpretation. Or, it could be that our models - or some of the ingredients therein - are the culprits.

The solar system ^3He data (meteorites, lunar soil and rocks, solar wind) have recently been reanalyzed by Geiss (1993) and by Copi, Schramm & Turner (1995). Although the size of the error estimates has increased compared, e.g., to those used in ST92, the central values remain unchanged. Consistency with our model predictions would require that the presolar ^3He abundance has been underestimated by more than a factor of 1.5-2.0.

The ISM data are more problematic. If, indeed, stellar production of new ^3He is occurring as indicated by the planetary nebulae observations (Rood, Bania & Wilson 1992; RBWB95), then X_3 should be higher where there is more stellar processing - in the inner galaxy. As may be seen in Figure 10, there is no observational evidence for such a trend. Indeed, the highest ^3He abundances are derived from data for the HII regions in the outer galaxy. The possibility that the ^3He abundances inferred from HII region radio observations are not reliable indicators of the current ISM values has also been invoked. Olive et al. (1995) have shown that unresolved structures in the nebulae may lead to an underestimate of their actual ^3He content but, only by a few tenths. On the other hand, the occurrence of a strong, ^3He depleted, Wolf-Rayet wind can reduce the ^3He abundance inside the HII region, although we presume that the external layers of many HII regions should still be uncontaminated and that a negative internal gradient should appear in the

abundances derived from central to outer parts within the nebulae observed with sufficient spatial resolution. Besides, if an HII region exhibits depleted ^3He because of the pollution from the central Wolf-Rayet star, it should also show enhanced ^4He , which does not seem to be the case for the RBWB95 sample. Olive et al. (1995) have tried to understand the ^3He distribution as a reflection of the mass of the HII regions (more destruction of ^3He in the more massive HII regions). This radical explanation makes little sense to us (and, to them as well) since it would require that HII regions are more efficient processors of interstellar material than the galaxy as a whole (since more than half the gas in these HII regions would have had to be cycled through the massive stars of the individual regions). Since the HII region data are hard to acquire and difficult to analyze (see, e.g., RBWB95), work on both fronts is important and, beyond the scope of our analysis here. So, here we have adopted the extant data, assumed that the inferred abundances are correct and investigated the implications for our models.

As may be seen in the Figures 8 & 9, the contribution from newly synthesized ^3He is large compared to the differences among the various model assumptions regarding the age of the disk, the infall abundances, the primordial abundances, the specific models (1, 25, NI). Therefore, the prime suspect must be our estimates of the ^3He yields from low and intermediate mass stars (Rood 1972 ; Galli et al. 1994; Hogan 1995; Wasserburg, Boothroyd & Sackmann 1995). To explore this avenue we have considered a series of non-standard alternatives to our standard models. Indeed, several suggestions have been published for physical mechanisms to suppress the overproduction of stellar ^3He . They are related to low-energy resonances or to deep convective mixing (e.g. Galli et al. 1994; Hogan 1995; Wasserburg, Boothroyd & Sackmann 1995), but none of them seems fully consistent with all the available data. In our cases II, III, VI and VIII the suppression of stellar produced ^3He may be sufficient to flatten the X_3 vs. t relation enough so that consistency with the local data may be found provided that the primordial abundances are small enough. However, it must be emphasized that if the detections of excess ^3He in planetary nebulae reported by Rood, Bania & Wilson (1992) and RBWB95 are confirmed, some of these alternatives (II and VI) are excluded. By comparing the model predictions with all the available constraints, we find that only case III is sufficiently compatible with all the data, despite its shallow negative gradient in the X_3 vs. R relation. In this case we may use the solar system data to bound the primordial abundance of ^3He from above and, the nucleon-to-photon ratio from below.

7. CONCLUSIONS

We have tracked the evolution of the abundances of D and ^3He in a variety of chemical evolution models which incorporate the results of a newly computed grid of stellar structure and evolution models. We have confirmed that D is fully destroyed during the pre-main sequence evolution and, therefore, its galactic evolution is simple. For the range of our models (see §3) we find only modest destruction of D and, using the solar system and

ISM data in concert with our “best” models, we bound the primordial (pre-galactic disk) abundance,

$$2.7 \leq 10^5 X_{2P} \leq 6.6, \quad 1.8 \leq 10^5 Y_{2P} \leq 4.4. \quad (1)$$

For consistency with the predictions of standard BBN (WSSOK), we require that the universal ratio of nucleons (baryons)-to-photons lie in the range,

$$4.1 \leq \eta_{10} \leq 7.1. \quad (2)$$

In terms of the baryon density parameter, Ω_B , ($\Omega_B h_{50}^2 = 0.015 \eta_{10}$; $H_0 = 50 h_{50}$ km/s/Mpc),

$$0.06 \leq \Omega_B h_{50}^2 \leq 0.10. \quad (3)$$

For our NI models the X_{2P} estimate is somewhat higher and the bounds on the baryon density slightly lower.

Our stellar models, which account for the evolution of ${}^3\text{He}$ (destruction, survival, production) reveal that for low mass stars the production of newly synthesized ${}^3\text{He}$ is very important for the evolution of galactic ${}^3\text{He}$. Indeed, for all of our standard models (§4) production of new ${}^3\text{He}$ is so dominant that even in the absence of any pre-galactic D and/or ${}^3\text{He}$, ${}^3\text{He}$ is overproduced compared to the solar system and ISM data. Until this conflict is resolved it is difficult to see how ${}^3\text{He}$ can be used as a probe of BBN (RST). Setting aside the possibility that the problem lies with the observational data, we have explored a series of non-standard models (§5) in which some or all of the newly synthesized ${}^3\text{He}$ is assumed to be destroyed before being returned to the ISM. We find that if this suppression of ${}^3\text{He}$ occurs only in stars $\leq 1 M_\odot$, the depletion is “too little, too late” to resolve the discrepancy with the solar system data. In contrast, ${}^3\text{He}$ destruction in stars with masses in the range 1-2 M_\odot (Wasserburg, Boothroyd & Sackmann 1995) can reconcile our models with the data provided that the initial ${}^3\text{He}$ abundance is not too large. In this case we recover a lower bound to the baryon density which is consistent with that derived from the D evolution data (see eqs. 1-3). It remains to be seen whether this “fix” will be permitted by the PNe and or ${}^{12}\text{C}/{}^{13}\text{C}$ data.

Acknowledgements

M.T. warmly thanks Letizia Stanghellini, Daniele Galli and Claudio Ritossa and G.S. thanks M. Pinsonneault for valuable and stimulating discussions. The work of G.S. is supported at Ohio State by the Department of Energy (DE-AC02-76-ER01545); part of this work was done while G.S. was a visitor at the Instituto Astronomico e Geofisico (Sao Paulo, Brasil) and he thanks them for hospitality and assistance.

REFERENCES

- Audouze, J. & Tinsley, B.M. 1974, ApJ, 192, 487
- Balsler, D.S., Bania, T.M., Brockway, C.J., Rood, R.T. & Wilson, T.L. 1994, ApJ, 430, 667
- Bahcall, J.N. & Ulrich, R.K. 1988, Rev. Mod. Phys., 60, 297
- Bania, T.M., Rood, R.T. & Wilson, T.L. 1987, ApJ, 323, 30
- Black, D.C. 1971, Nature Phys. Sci., 234, 148
- Black, D.C. 1972, Geochim. Cosmochim. Acta, 36, 347
- Bolte, M. 1994, ApJ, 431, 223
- Carswell, R.F., Rauch, M., Weymann, R.J., Cooke, A.J. & Webb, J.K. 1994 MNRAS, 268, L1
- Charbonnel, C. 1995, preprint
- Dearborn, D.S.P. 1992, Phys. Rep., 210, 367
- Dearborn, D.S.P. & Eggleton, P.P. 1976, QJRAS, 17, 448
- Dearborn, D.S.P., Griest, K. & Raffelt, G. 1991, ApJ, 368, 626
- Dearborn, D.S.P., Schramm, D.N. & Steigman, G. 1986, ApJ, 203, 35 (DSS)
- Edmunds, M.G. 1994, MNRAS, 270, L37
- Eggleton, P.P. 1967, MNRAS, 135, 243
- Eggleton, P.P. 1968, MNRAS, 143, 87
- Fields, B.D. 1995, ApJ, In Press
- Galli, D., Palla, F., Ferrini, F. & Penco, U. 1995, ApJ, 443, 536
- Galli, D., Palla, F., Straniero, O. & Ferrini, F. 1994, ApJ, 432, L101
- Geiss, J. 1993 in *Origin and Evolution of the Elements*, N.Prantzos, E.Vangioni-Flam and M.Cassé eds. (CUP, U.K.), p.89
- Geiss, J. & Reeves, H. 1972, A&A, 18, 126
- Giovagnoli, A. & Tosi, M. 1995, MNRAS, 273, 499
- Hogan, C.J. 1995, ApJ, 441, L17
- Huebner, W.F., Merts, A.L., Magee, N.H.Jr., & Argo, M.F. 1977, Astrophysical Opacity Library (LASL, LA-6760-M)

Iben, I.Jr. 1967, ApJ, 147, 624

Iglesias, C. A. & Rogers, F. J. 1990 , ApJ, 360, 221

Iglesias, C. A. & Rogers, F. J. 1992 , ApJ, 397, 717

Linsky, J.L., Brown, A., Gayley, K., Diplas, A., Savage, B.D., Ayres, T.R., Landsman, W., Shore, S.W. & Heap, S. 1993, ApJ, 402, 694

Matteucci, F. & François, P. 1989, MNRAS, 239, 885

Olive, K.A., Rood, R.T., Schramm, D.N., Truran, J. & Vangioni-Flam, E. 1995, ApJ, 444, 680

Olive, K.A. & Steigman, G. 1995, ApJS, 97, 49

Pagel, B.E.J., Simonson, E.A., Terlevich, R.J. & Edmunds, M.G. 1992, MNRAS, 255, 325

Prantzos, N. 1995, A&A In Press

Rood, R.T. 1972, ApJ, 177, 681

Rood, R.T., Bania, T.M. & Wilson, T.L. 1992, Nature, 355, 618

Rood, R.T., Bania, T.M., Wilson, T.L. & Balser, D.N. 1995 in *The Light Element Abundances*, P.Crane ed. (Springer-Verlag), p. 201, RBWB95

Rood, R.T., Steigman, G. & Tinsley, B.M. 1976, ApJ, 207, L57, RST

Scully, S.T. & Olive, K.A. 1995, ApJ, In Press

Skillman, E.D., Terlevich, R.J., Kennicutt, R.C., Garnett, D.R. & Terlevich, E. 1994, ApJ, 431, 172

Songaila, A., Cowie, L.L., Hogan, C.J., & Rugers, M. 1994, Nature, 368, 599

Spite, F. & Spite, M. 1982, A&A, 115, 357

Steigman, G. 1994, MNRAS, 269, P53

Steigman, G. & Tosi, M., 1992, ApJ, 401, 150, ST92

Steigman, G. & Tosi, M., 1995, ApJ, 453, 173

Thomas, D., Hata, N., Scherrer, R., Steigman, G. & Walker, T. 1996, In Preparation

Thorburn, J. 1994, ApJ, 421, 318

Tinsley, B.M. 1980, Fund.Cosmic Phys., 5, 287

Tosi, M., 1988a, A&A, 197, 33

Tosi, M., 1988b, A&A, 197, 47

- Tosi, M., Steigman, G. & Dearborn, D.S.P. 1994, in *The Light Element Abundances*, P.Crane ed. (Springer-Verlag), p.228
- Tytler, D. 1995 in *QSO Absorption Lines*, G.Meylan ed. (Springer-Verlag) In Press
- Vangioni-Flam, E. & Audouze, J. 1988, A&A, 193, 81
- Vangioni-Flam, E., Olive, K.A. & Prantzos, N. 1994, ApJ, 427, 618
- Vassiliadis, E. & Wood, P.R. 1993, ApJ, 413, 641
- Walker, T.P., Steigman, G., Schramm, D.N., Olive, K.A. & Kang, H.S. 1991, ApJ, 376, 51, WSSOK
- Wannier, P.G. 1980, ARA&A, 18, 399
- Wasserburg, G., Boothroyd, A. & Sackmann, I.-J., 1995, ApJ, 447, L37
- Yang, J., Turner, M.S., Steigman, G., Schramm, D.N. & Olive, K.A. 1984, ApJ, 281, 493, YTSSO

FIGURE CAPTIONS

Figure 1. Top panel: final envelope abundance of ${}^3\text{He}$ as a function of the stellar initial mass for five different main sequence abundances of ${}^3\text{He}$ and $Z=0.02$. Bottom panel: final envelope abundance of ${}^3\text{He}$ as a function of the stellar initial mass for three different metallicities and $X_{3,MS} = 2.1 \times 10^{-4}$.

Figure 2. Final envelope abundance of ${}^3\text{He}$ for $Z=0.02$ in stars of initial mass $M/M_{\odot}=1, 3, 8$ and 100 as a function of the main sequence abundance.

Figure 3. Survival fraction g_3 of ${}^3\text{He}$ as a function of the stellar initial mass for $Z=0.02$ and five different main sequence abundances of ${}^3\text{He}$.

Figure 4. Average g_3 convolved with Tinsley’s (1980) IMF as a function of the lower mass limit m_l on the IMF integral.

Figure 5. Deuterium survival factor f_2 as a function of time predicted by different models of the solar ring ($R= 8$ kpc). Models shown in the left panel assume 13 Gyr for the current age of the galactic disk; those in the right panel assume 10 Gyr. In both panels, dotted curves correspond to no infall models, solid curves to models 1 (upper curve) and 25 (lower curve) with $X_{2infall} = 0.8X_{2P}$, dashed curves to models 1 (upper curve) and 25 (lower curve) with $X_{2infall} = X_{2P}$.

Figure 6. Evolution in the solar ring of the D abundance. Vertical bars give the 2σ range for the abundances derived from solar system and local ISM observations (see text). Left panels correspond to a disk age of 13 Gyr, right panels to 10 Gyr. Models in the top panels assume the maximum value of primordial D consistent with the data; models in the bottom panels the corresponding minimum value. The dash-dotted lines correspond to “standard” models with primordial infall (1-B-Ia and 1_{10} -B-Ia), the other symbols are as in Fig.5

Figure 7. Current radial distribution of the D abundance resulting from the same models as Fig.5 (same symbols as in that figure). In each pair of curves of the same line-type, the steeper one corresponds to model 1 and the flatter one to model 25. Data points are from Wannier (1980) but arbitrarily divided by 100.

Figure 8. Evolution of the ${}^3\text{He}$ abundance in the solar ring as predicted by models 1. The vertical bars show the 2σ range for the solar system and ISM abundances (see text for details). In the top panel all models adopt the standard stellar yields (see Sec.2 and Table 1) and assume primordial infall. They are in order of decreasing ${}^3\text{He}$ and D abundances (i.e. from top to bottom): 1-R-Ia, 1-J-Ia, 1-W-Ia, 1-I-Ia, 1-X-Ia, 1-H-Ia, 1-M-Ia. The models in the lower panel all start with the same primordial abundances of D and ${}^3\text{He}$ but have different adopted stellar yields and infall metallicity. From top to bottom they are: 1-W-(Ic, Ia, Ib, Id, Vb, VIIIb, IIIb, VIb).

Figure 9. Evolution of the ${}^3\text{He}$ abundance in the solar ring as predicted by different chemical evolution models (1, 25, NI) using the same stellar yields and infall metallicity.

The left-hand panel corresponds to a disk age of 13 Gyr and the right-hand panel to 10 Gyr. The lower and upper solid lines are models 1-T-IIIb and 25-T-IIIb respectively (see Table 1); the lower and upper dashed lines are models 1-H-VIIIb and 25-H-VIIb; the dotted line is for NI-Z-III.

Figure 10. Predicted current radial distribution of the ${}^3\text{He}/\text{H}$ number ratio. Data points and error bars are from the HII region analysis by RBWB95 and the specific models are labelled.

Table 1. Models and Initial Abundances.

Model ¹	$10^5 X_{2p}$	$10^5 X_{3p}$	Model ¹	$10^5 X_{2p}$	$10^5 X_{3p}$
Models with standard ^3He evolution and primordial infall					
1-M-Ia	0.0	0.0	1-K-Ia	4.0	1.0
1-A-Ia	2.5	2.0	1-O-Ia	4.5	0.0
1-H-Ia	3.0	0.0	1-C-Ia	5.0	2.0
1-I-Ia	3.0	2.0	1-X-Ia	6.0	0.0
1-B-Ia	3.0	2.5	1-W-Ia	6.0	2.0
1-J-Ia	3.0	4.0	1-R-Ia	6.0	4.0
1-L-Ia	3.85	0.0	1 ₁₀ -B-Ia	3.0	2.5
Models with standard ^3He evolution and non-primordial infall					
1-K-Ib	4.0	1.0	1-W-Ib	6.0	2.0
1-K-Ic	4.0	1.0	1-W-Ic	6.0	2.0
1-K-Id	4.0	1.0	1-W-Id	6.0	2.0
1-C-Ib	5.0	2.0	1-W-Ie	6.0	2.0
Models with non-standard ^3He evolution and primordial infall					
1-T-IIIa	6.0	1.5	25-T-IIIa	6.0	1.5
1 ₁₀ -T-IIIa	6.0	1.5	25 ₁₀ -T-IIIa	6.0	1.5
Models with non-standard ^3He evolution and non-primordial infall					
1-H-VIIIb	3.0	0.0	1-Q-IIIb	6.0	3.0
1-K-Vd	4.0	1.0	1-Q-Vb	6.0	3.0
1-K-VIIIb	4.0	1.0	1-U-VIb	6.0	3.5
1-V-Vb	5.0	0.0	1-R-VIb	6.0	4.0
1-S-Vb	5.0	1.0	1 ₁₀ -H-VIIIb	3.0	0.0
1-C-IIb	5.0	2.0	1 ₁₀ -C-VIb	5.0	2.0
1-C-IIIb	5.0	2.0	1 ₁₀ -T-IIIb	6.0	1.5
1-C-IVb	5.0	2.0	1 ₁₀ -W-VIIIb	6.0	2.0
1-C-Vb	5.0	2.0	25-H-VIIIb	3.0	0.0
1-C-VIb	5.0	2.0	25-K-VIIIb	4.0	1.0
1-C-VII	5.0	2.0	25-C-VIb	5.0	2.0
1-C-VIIIb	5.0	2.0	25-C-VIIIb	5.0	2.0
1-T-IIIb	6.0	1.5	25-T-IIIb	6.0	1.5
1-T-Vb	6.0	1.5	25 ₁₀ -H-VIIIb	3.0	0.0
1-W-IIb	6.0	2.0	25 ₁₀ -T-IIIb	6.0	1.5
1-W-IIIb	6.0	2.0	NI-C-III	5.0	2.0
1-W-Vb	6.0	2.0	NI-Z-III	9.0	1.5
1-W-VIb	6.0	2.0	NI ₁₀ -C-III	5.0	2.0
1-W-VIIIb	6.0	2.0	NI ₁₀ -Z-III	9.0	1.5

¹Arabic numbers refer to the type of chemical evolution model (see text and Tosi 1988a). Capital letters indicate the adopted primordial abundances. Roman numerals indicate the stellar yields adopted for ^3He : I, as described in section 2; II, as for Model I but with $g_3=1$ for $M < 2 M_\odot$; III, as for Model I but with $g_3=1$ for stars with $1 < M/M_\odot < 2$; IV, as for Model I but with total ^3He destruction in stars with $M \leq 1 M_\odot$; V, following Pinsonneault (1995); VI, following Hogan (1995); VII, as for Model VI but with ^3He destruction for $M \leq 1.6 M_\odot$; VIII, as for Model VI but with ^3He destruction in the range $1.3 < M/M_\odot < 2.5$. Lower case letters indicate the adopted infall abundances: a, $X_{2inf}=X_{2p}$ and $X_{3inf}=X_{3p}$; b, $X_{2inf}=0.8X_{2p}$ and $X_{3inf}=X_{3p}$; c, $X_{2inf}=0.8X_{2p}$ and $X_{3inf}=1.2X_{3p}$; d, $X_{2inf}=0.8X_{2p}$ and $X_{3inf}=0.8X_{3p}$; e, $X_{2inf}=0.7X_{2p}$ and $X_{3inf}=X_{3p}$.

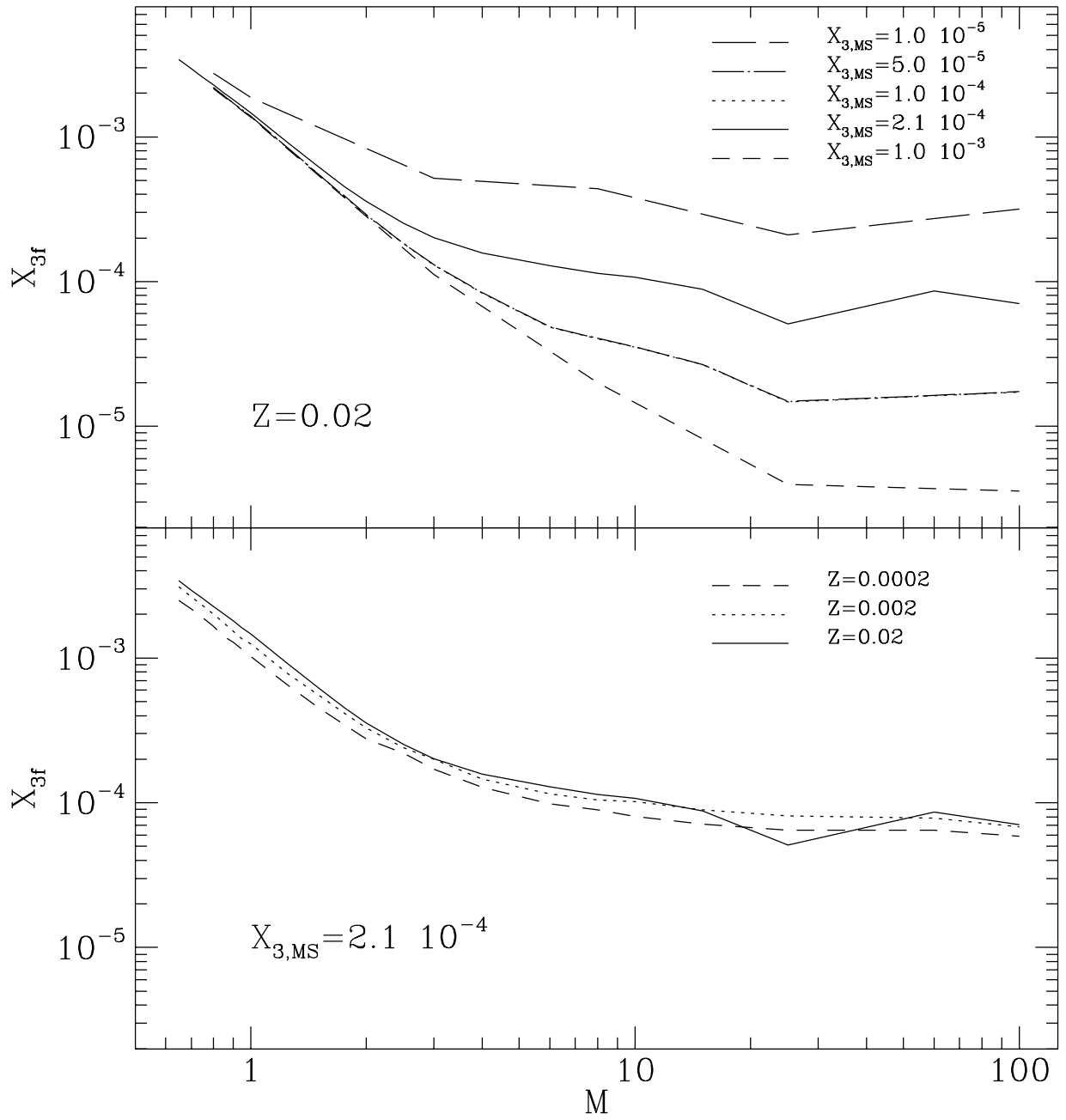


Figure 1

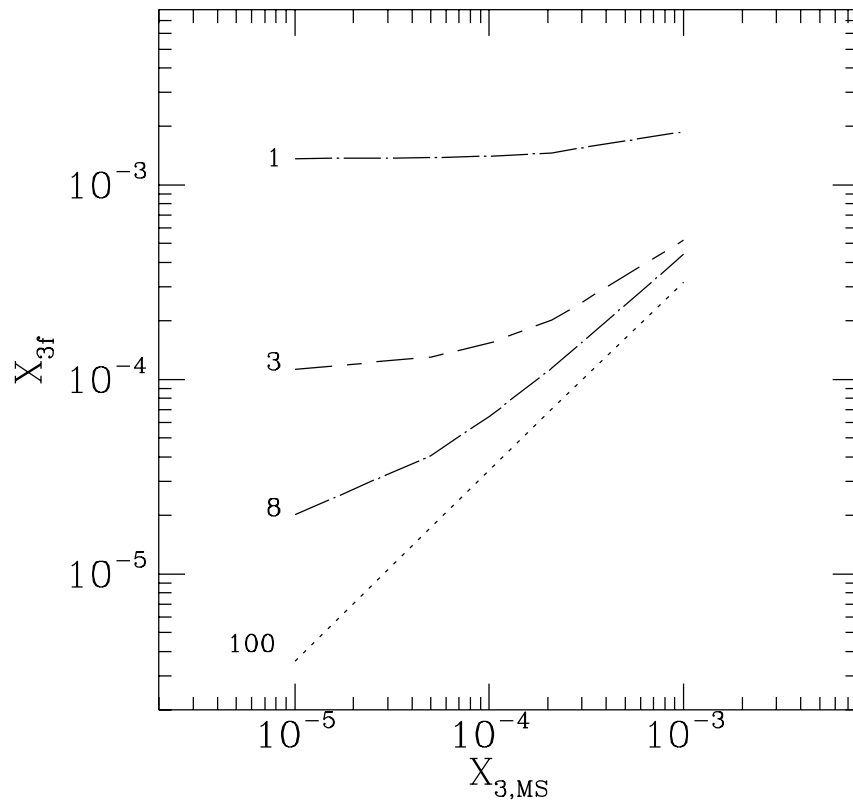


Figure 2

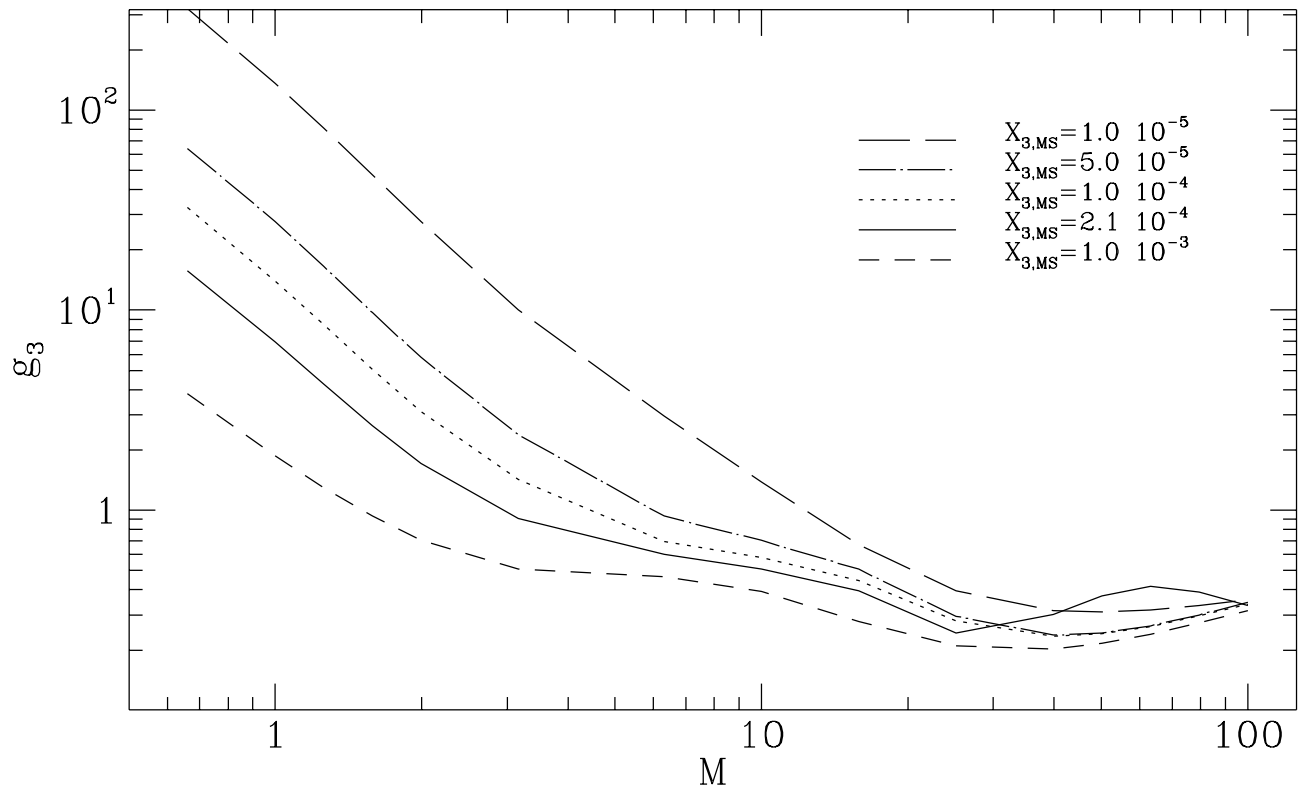


Figure 3

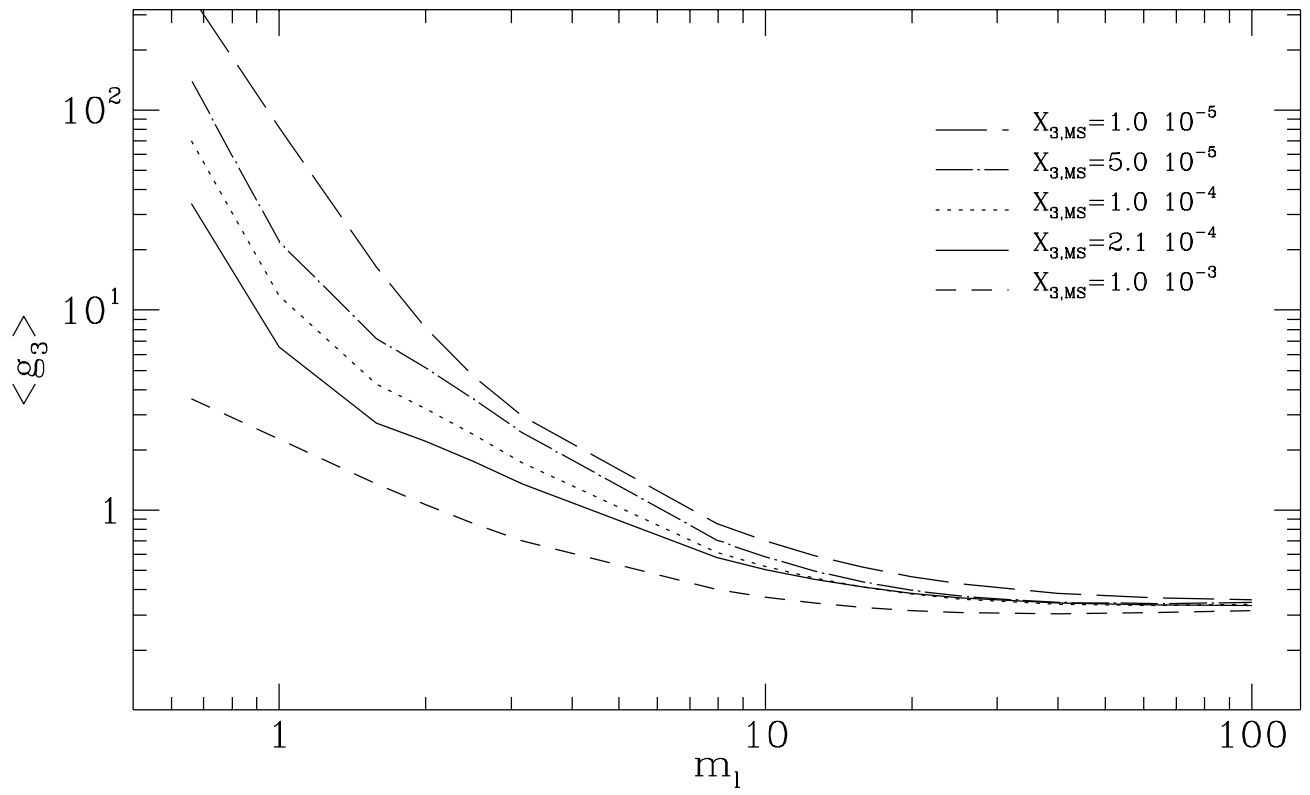


Figure 4

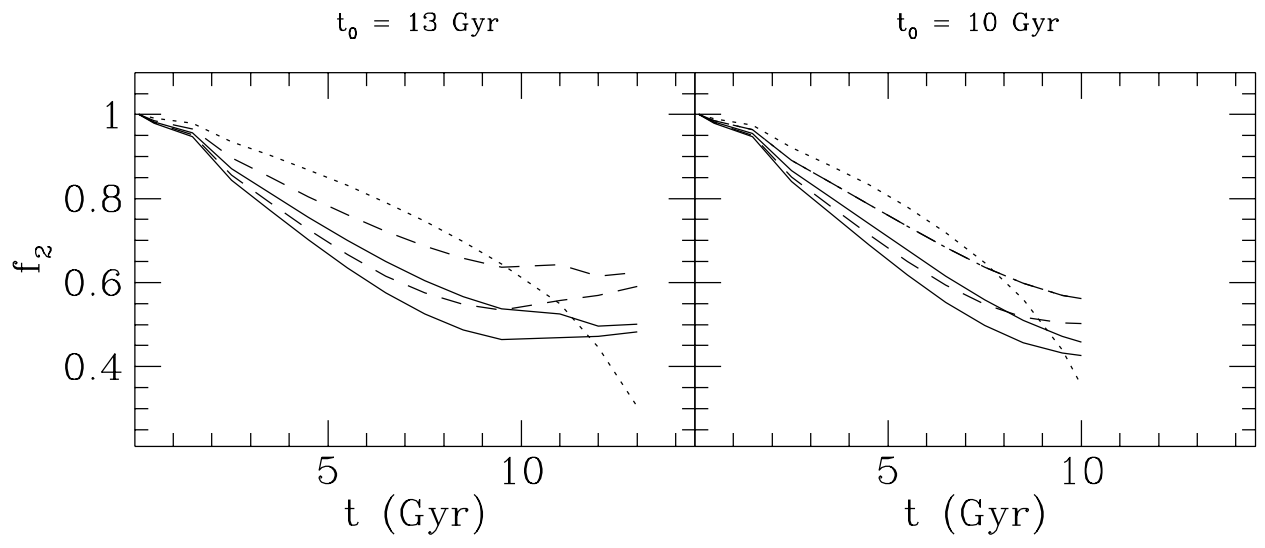


Figure 5

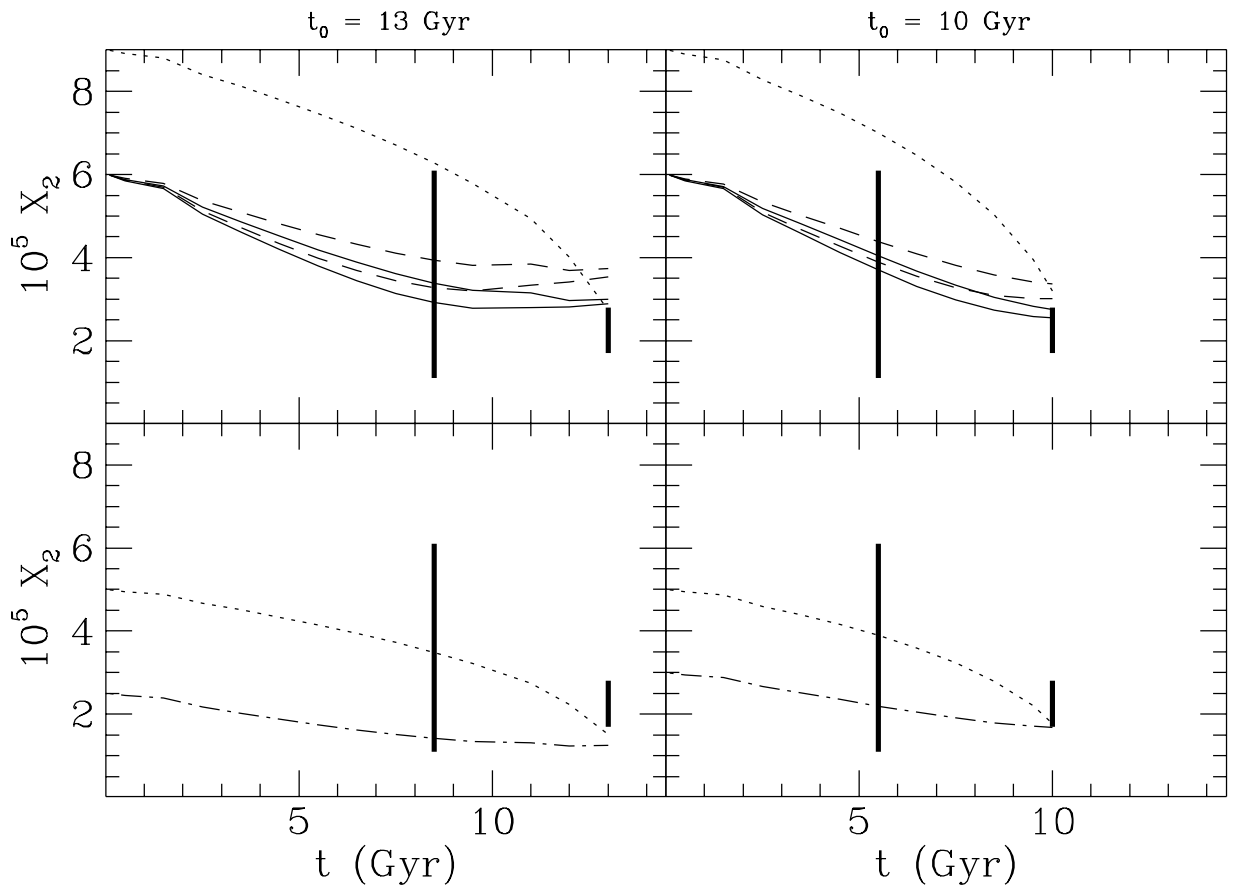


Figure 6

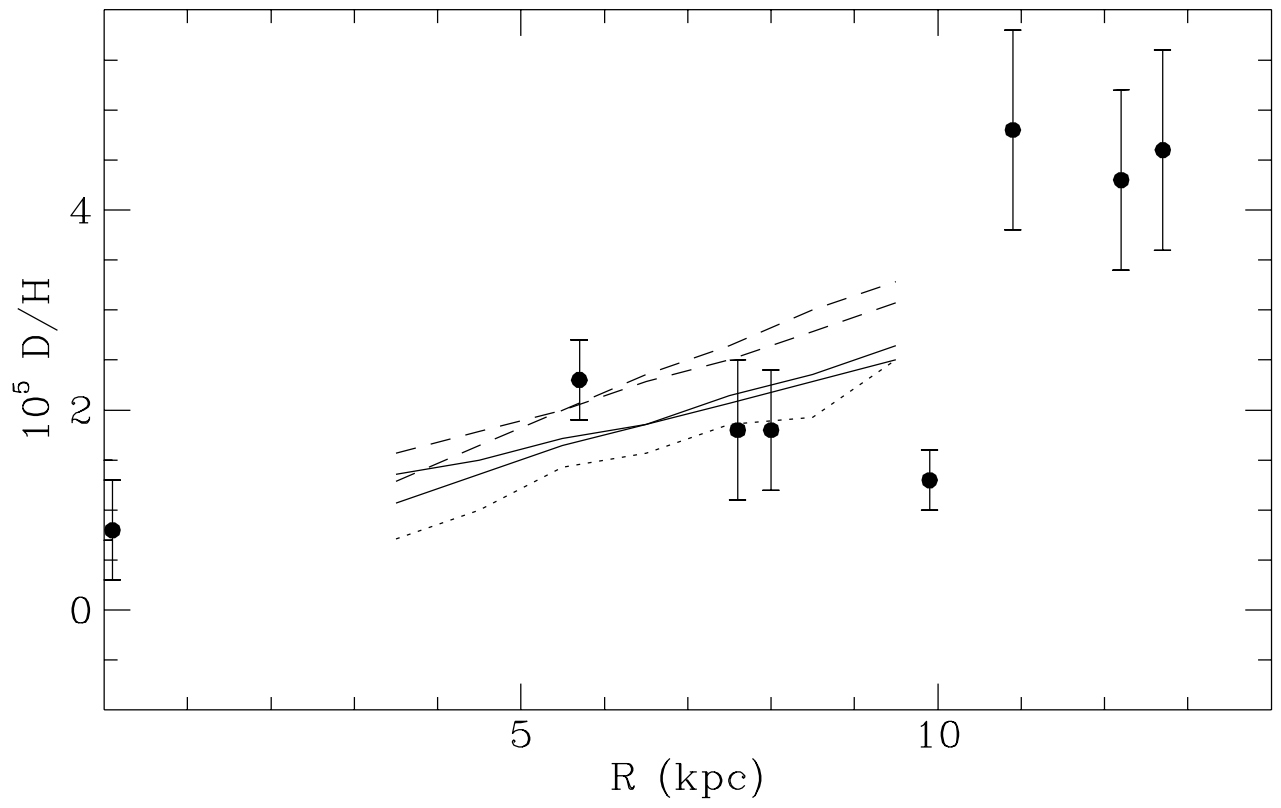


Figure 7

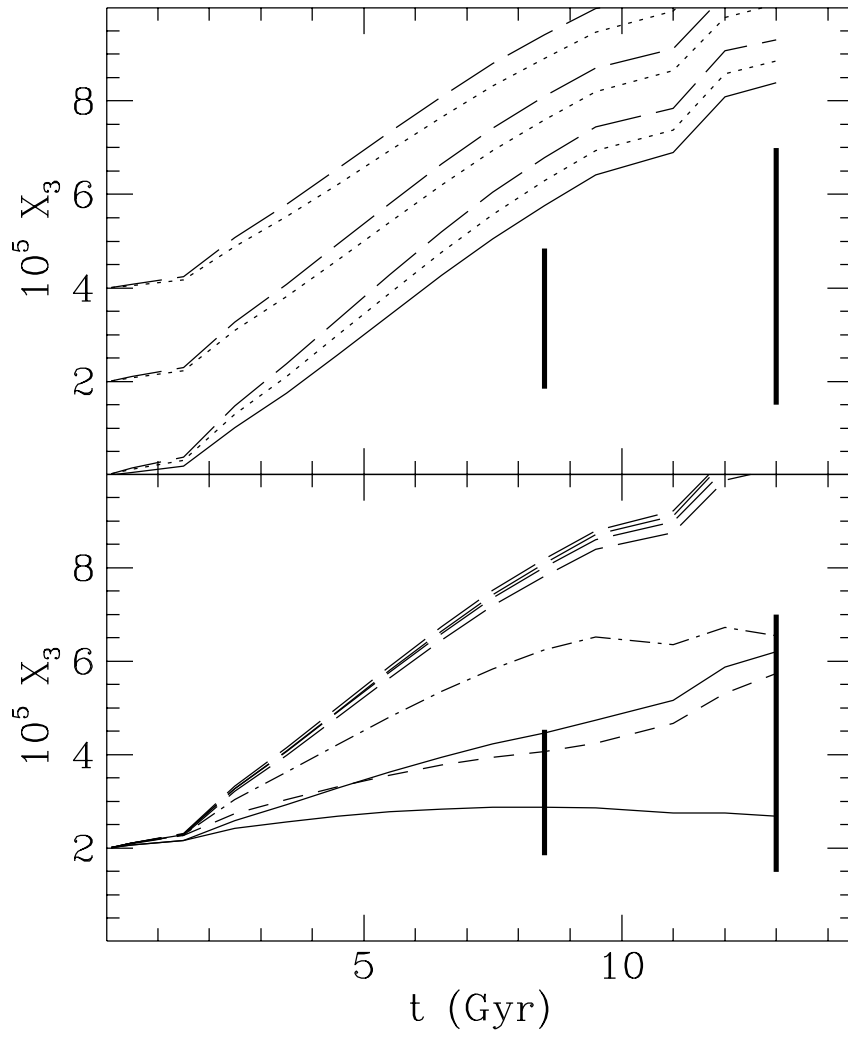


Figure 8

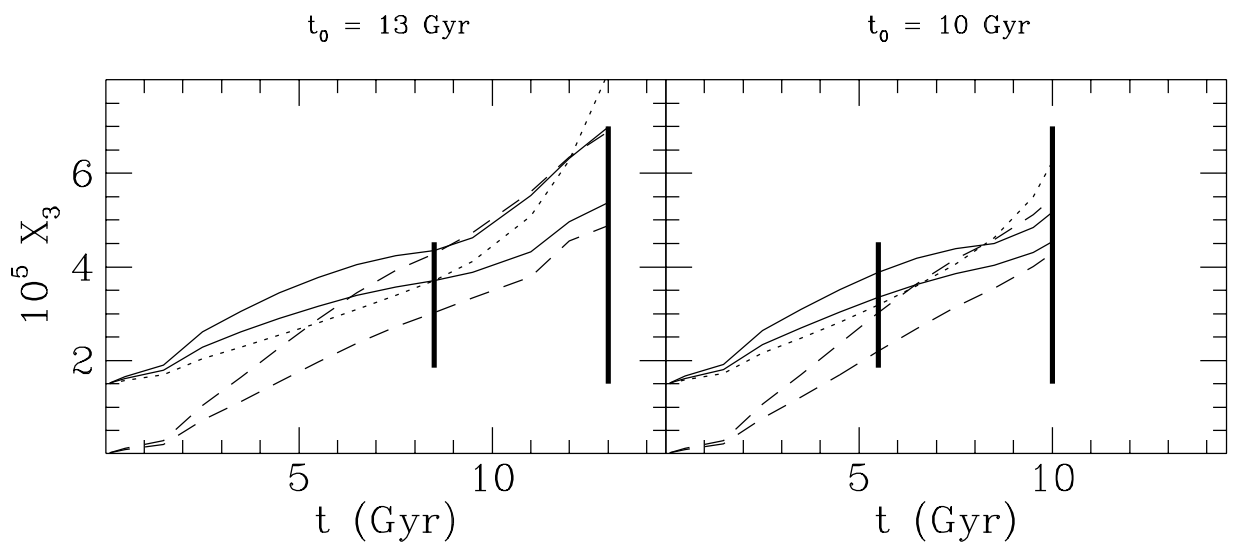


Figure 9

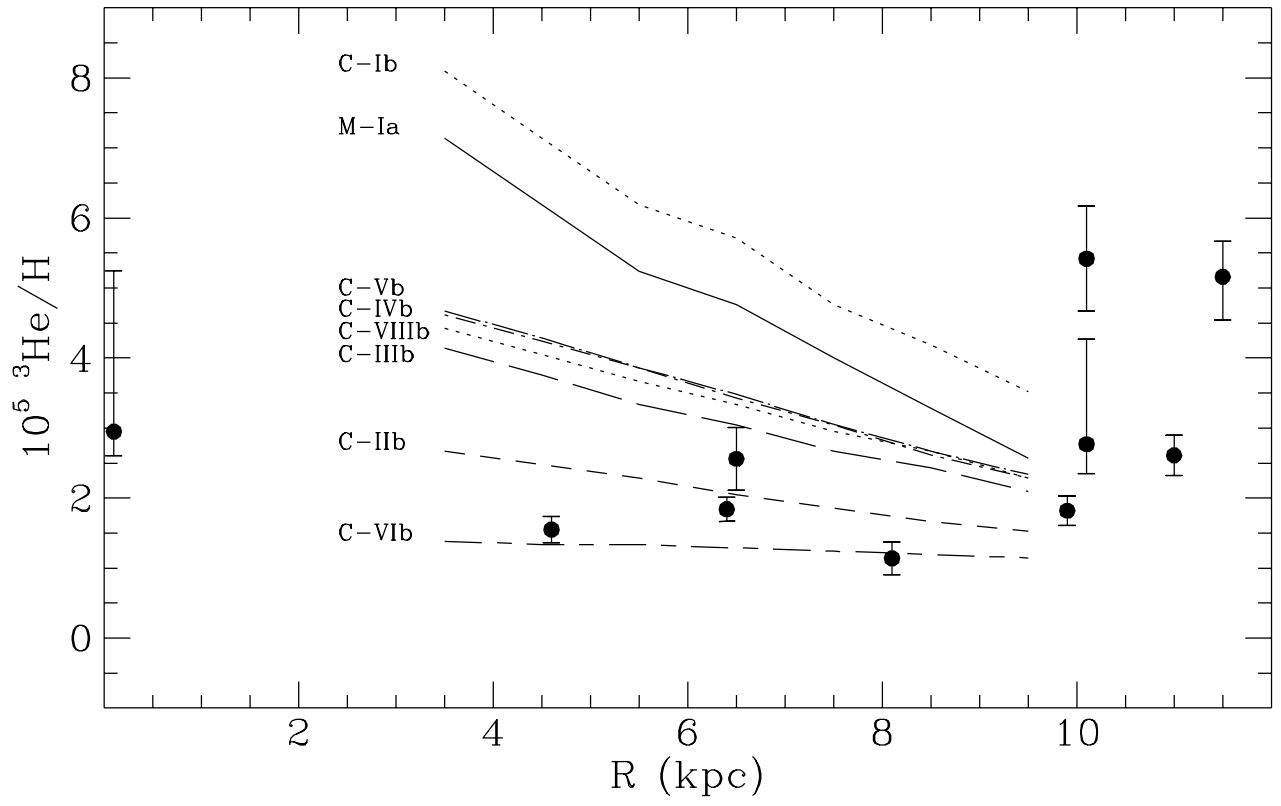


Figure 10